Data-driven modelling of vertical dynamic excitation of bridges induced by people running

Vitomir Racic [a,*], Jean Benoit Morin [b]

[a] Department of Civil & Structural Engineering, University of Sheffield, Sir Frederick Mappin Building, Sheffield S1 3JD, UK
[b] Faculty of Science and Technology, Université Jean Monnet, Saint-Etienne, France

Article history:
Received 29 January 2013
Received in revised form
25 June 2013
Accepted 6 October 2013
Available online 2 November 2013

1. Introduction

In the last 15 years substantial developments in workmanship and structural materials have enabled bridge engineers to promote much more slender designs than ever. These reduce the mass and stiffness of the structure, hence the bridge is more likely to have a natural frequency well below 5 Hz for spans greater than 50 m [1]. As a result, modern bridges are at a considerable risk of developing resonance when occupied and dynamically excited by people moving during ordinary activities, such as walking, jumping and running [2]. Excessive dynamic responses recorded worldwide on at least a

* Corresponding author. Tel.: +44 114 222 5790; fax: +44 114 222 5718.
E-mail address: v.racic@sheffield.ac.uk (V. Racic).

Nomenclature

f_r	footfall rate or running frequency
$F(t)$	force–time history
G	body weight
α_i	dynamic load factors (DLF)
φ_i	Fourier phases
f_s	sampling rate
T_i, $T_k^{'}$	cycle intervals
τ_i, $\tau_k^{'}$	normalised cycle intervals
μ_T	mean of T_i
$S_\tau(f_m)$, $S_\tau^{'}(f_n)$, $S_\tau^{'}(f)$	ASD of τ_i and $\tau_k^{'}$
A_τ	Fourier amplitudes of τ_i
A_j, W_j	Gaussian heights (weights)
t_j, c_j	Gaussian centres
δ_j, b	Gaussian widths
$Z(t)$	template cycle
E_i, $E_k^{'}$	energy of weight normalised cycles
E_{tc}	energy of template cycle
ΔE_i	disturbance term
ξ_k	scaling factor
ρ_0, ρ_1	coefficients of linear regression
ρ	coefficients of linear correlation
N	number of cycles
T	duration of force signal

dozen bridges of different structural forms and sizes under groups and crowds of active people clearly prove the point [3–10].

While the loads induced by walking [6–8,11–13] and jumping [10,14] have been intensively studied, reliable and practical descriptions of running forces (including jogging and sprinting) are still very rare and limited. One of the first single-footfall measurements was conducted by Galbraith and Barton [15] who used a force plate. Measurements of individual step forces were followed by more advanced and informative measurement of continuous running time histories comprising several steps. For this purpose Rainer et al. [16] used a continuously measured reaction of a floor strip having known dynamic properties, while more recently Sahnaci and Kasperski [17] used an instrumented walkway. However, both facilities could record forces for a maximum of four successive footfalls, which is far below the 32–64 successive footfalls necessary for statistically reliable analysis of running time series [18]. Much research into running forces has been in the domain of biomechanics as the contact forces between the feet and supporting ground (thus generally called "ground reaction forces" – GRFs) provide useful diagnostics for medical and sports applications [19]. Medics introduced instrumented force measuring treadmills which can be used to carry out even high-speed running studies in very small laboratories [18]. However, no database of running forces in the form of continuously recorded signals has yet been found that can be used for development of their statistically reliable characterisation for application in the civil engineering context.

The lack of fundamental forcing data and their reliable mathematical models has resulted in a total lack of formal design guidance regarding running excitation of bridges. As a result, bridge designers are faced nowadays with a great deal of uncertainty about dynamic performance of the structure under a number of relevant loading case scenarios related to people running, such as increasingly popular marathon events in urban environments [9,20]. The present study aims to change this situation by bringing together: (1) a comprehensive database of continuously measured vertical running loads generated by individuals on flat stationary surfaces (i.e. without the vertical bridge motion and hence discounting effects of human–structure dynamic interaction), and (2) two mathematical characterisations of the measurements. The first modelling strategy is based on a deterministic perfectly periodic Fourier-based approach adapted from a popular design guideline for walking loading [20], while the second model features more realistic stochastic-based modelling of narrow-band signals. The models could be applied to cases of incipient instability, i.e. when vertical bridge motion is still not significantly perceptible to the runner, and is ideally suited for considering cases of multiple runners in a group or crowd.

Realistic modelling of running force signals, based on direct observation and measurement, is an essential prerequisite to predicting bridge vibrations whether or not they are perceptible. McMahon and Greene [21] showed that a decrease in surface stiffness resulted in a decrease in a runner's metabolic rate and a decrease in the vertical GRF, but without affecting running mechanics. Also, there is strong evidence that peripheral stimuli are an equally important factor influencing timing of footfalls [9] and that resulting GRFs are inevitably a narrow-band random process [22]. Hence, the present study focuses on appropriate modelling of this process in order to build a framework that can generate the correct interface forces between the runners and the structure.

2. Definition of running

Of all factors that influence running GRFs, such as the body morphology [23], gait style [24], mechanical properties of the supporting surface [25], texture and stiffness of footwear [26], speed is the most prominent [27]. Typical running force-time history is a series of pulses separated by zero-force periods, which correspond to the "flying" phase of running when both feet are off the ground (Fig. 1a). In contrast, during walking only one foot at a time leaves contact with the ground and there is a period of double-support (Fig. 1b). Running footfalls also have one dominant peak and therefore differ from the characteristic double-peak shape (also called "M shape") of walking footfalls. Hence, people walking and running clearly represent two different dynamic loading case scenarios of footbridges.

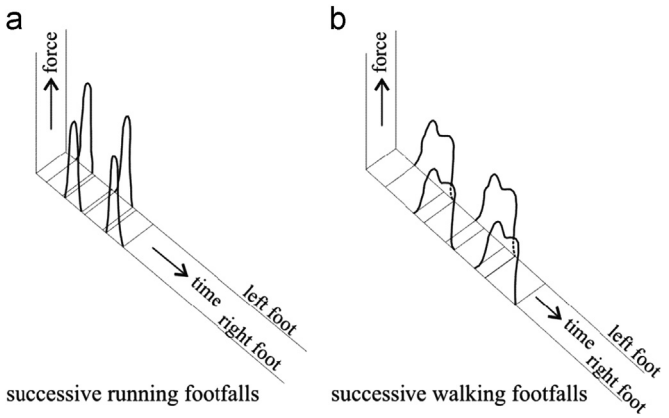

Fig. 1. (a) Running and (b) walking footfalls (after Galbraith and Barton [15]).

There is some evidence from both measurements of oxygen consumption [28] and mechanical simulations of bodies in motion [29] that people select gait style at a given speed to optimise energy cost of locomotion. In fact, walking feels easiest at low speeds and running feels easiest at fast speeds [30]. Hence people switch from a walk to run at speeds close to the boundary at which walking ceases to be optimal [31,32]. However, in the proximity of this boundary both fast walking and slow running (i.e. jogging) are possible. From the perspective of bridge dynamics, jogging is potentially more severe loading scenario than walking since it is characterised by more bouncy (i.e. trotting) gait style yielding higher force amplitudes. The difference is illustrated in Fig. 2.

In the present study, all test subjects were encouraged to start jogging at the slowest possible but still comfortable speed, i.e. self-selected speed at which jogging feels natural. The test protocol is elaborated in the next section.

3. Experimental data collection

A database comprising many force records at a wide range of running speeds (i.e. from jogging to sprinting) is an essential component for their mathematical characterisation presented in Sections 4 and 6. In this paper, such a database is established using two force measuring treadmills, as elaborated in Sections 3.1 and 3.2.

Although there is no theoretical difference in the physics of treadmill and overground locomotion, some early experimental studies reported major discrepancies [33]. The reason for this was thought to be imposed "constant" speed of movement, controlled by rotation of the treadmill belt, as opposed to the overground locomotion when the gait speed has no similar control [34]. However, van de Putte et al. [35] and Riley et al. [36] showed more recently that difference between treadmill and overground locomotion is negligible for those who use treadmill regularly (e.g. to maintain fitness). In addition, based on a statistical comparison between three-dimensional knee kinematics and step lengths recorded on ten healthy test subjects, van de Putte et al. [35] showed that habituation of inexperienced test subjects to treadmill locomotion takes up to 10 min. These studies demonstrated the essential equivalence between treadmill and overground locomotion in biomechanical domain, such as measuring performance of healthy athletes [37] and design of "blade runners" for disabled athletes [38]. Hence, they justify treadmill-based force measurements in design of less delicate bridge structures.

3.1. Experimental setup

The tests were carried out in the Vibration Engineering Section Laboratory in the University of Sheffield (UK) and Laboratoire de Physiologie de l'Exercice in the University Jean Monnet Saint-Etienne (France). Continuously measured individual force records were collected on two state-of-the-art instrumented treadmills: ADAL3D-F in Sheffield (Fig. 3a) and ADAL3D-R in France (Fig. 3b).

All components of each treadmill, including brushless servo motors equipped with internal velocity controllers, belts and secondary elements, are mounted on a rigid metal frame and mechanically connected to the supporting ground only through four Kistler 9077B three-axial piezoelectric force sensors [39]. These transducers have high stiffness to avoid any possibility of system dynamic characteristics affecting measurements. The whole system is mechanically isolated, i.e. the sensors measure only external running forces, while the internal forces due to belt friction and belt rotation are not detected by the sensors [18]. More technical details and a full description of the force measuring process are elaborated in ADAL3D user manuals [40].

Speed of the belt rotation (here also called "treadmill speed") can be controlled and monitored remotely either with a control panel or with bespoke software, run from the data acquisition PC. Similar to fitness treadmills, the remote control panel and the treadmill itself are equipped with a safety stop switch. Rotational speed of ADAL3D-F belts is in the

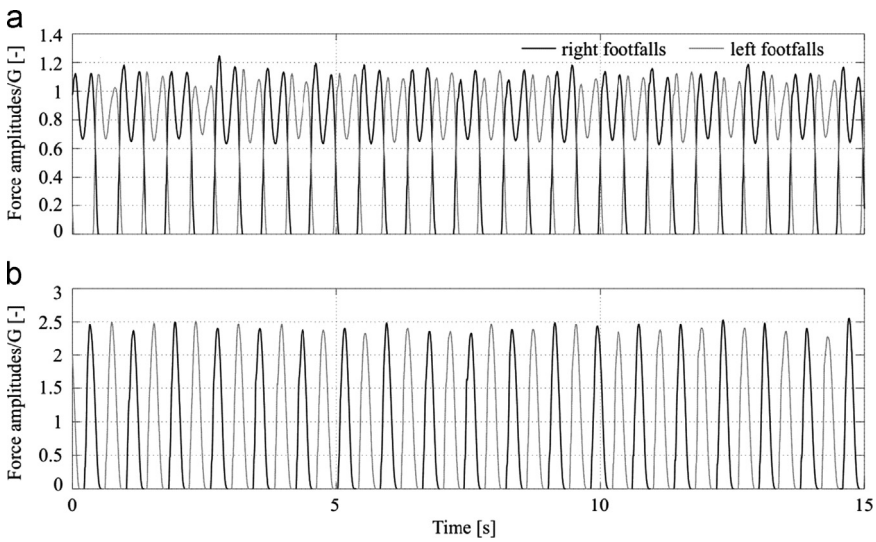

Fig. 2. Force signals generated by the same individual (a) walking and (b) jogging at 8 km/h.

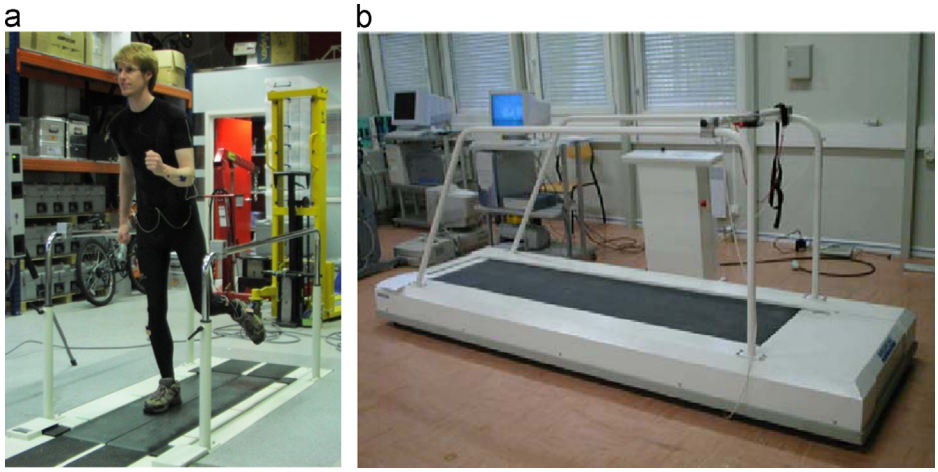

Fig. 3. Experimental setup in (a) Sheffield and (b) Saint-Etienne.

range 0.1–10 km/h, whereas the speed range of ADAL3D-R is extended up to 25 km/h. The difference in speed range gave rise to different test protocols used in Sheffield and Saint-Etienne, as elaborated in the next section.

3.2. Test sequence

Prior to the force measurements, the Research Ethics Committee of the University of Sheffield and the University Jean Monnet Saint-Ettiene required each prospective test subject complete a Physical Activity Readiness Questionnaire and pass a preliminary fitness test (by satisfying predefined criteria for blood pressure and resting heart rate) to check whether they were suited for physical activity required during the experiment. Measurements of the body mass, age and height were taken for test subject who passed the preliminary test.

All participants wore comfortable running footwear. Those who had no experience with treadmill running were given a brief training prior to the force collection supervised by a qualified instructor. Each participant had at least 10 min long warming up, which included walking and jogging on the treadmill while the speed was varied randomly and controlled by the speed of rotation of the treadmill belts.

During each individual test participants were asked to run on the treadmill at a fixed speed, which was the average individual's running speed. The latter could vary on the step-by-step basis around the given treadmill speed as 1 m long belts allowed test subjects to move forwards and backwards on the treadmill, thus to slow down and speed up while

running. This made running feel natural and allowed variability of footfalls normally present in overground running [35]. Pacing rate was not prompted by any stimuli such as a metronome, and it was determined only from subsequent analysis of the generated force signals (see Section 4). Each test was completed when at least 64 successive footfalls were recorded. Rests were allowed between successive tests.

In Sheffield, acquisition of the force records started at the slowest self-selected speed at which jogging, rather than walking, is more comfortable. In the 95% of cases processed, this speed was 7 km/h, after being rounded to nearest integer. In each following test the running speed was increased by 0.5 km/h, until it added up to 10 km/h. In Saint-Ettiene, the first test was run at 10 km/h and the speed was increased by 0.5 km/h in each following test until a participant reached either their maximum sprinting speed or 25 km/h. All recorded force signals were sampled at 200 Hz.

In total, 45 volunteers (30 males and 15 females, body mass 72.3 ± 14.2 kg, height 175.2 ± 7.1 cm, age 27.2 ± 8.1 years) were drawn from students, academics and technical staff of the University of Sheffield and the University Jean Monnet Saint-Ettiene. All together they generated 458 vertical running force–time histories of kind illustrated in Fig. 2b. In the remaining part of the paper, this unique database is used to provide their first mathematical representations derived from the actual continuously measured force records. Section 4 takes a traditional yet conservative approach to modelling human-induced dynamic loading based on the deterministic representation of their dominant Fourier harmonics [41,42]. On the other hand, Section 5 presents a radically different model motivated by the existing numerical generators of earthquakes [43], human electrocardiogram signals [44] and speech recognition [45] which can accurately simulate the measurements.

4. Modelling approach based on Fourier series

Measured force–time histories of human-induced loading are invariably near-periodic [22], indicating their narrow band nature (Fig. 4b). However, to simplify their mathematical representations for design purposes, they are usually assumed perfectly periodic, deterministic and presentable via Fourier series:

$$F(t) = G \sum_{j=1}^{m} \alpha_i \sin(2\pi i f_r t - \varphi_i) \tag{1}$$

Here $F(t)$ represents the total force at time t, with G representing the body weight in the same unit. A total of m harmonics are considered, capturing peaks α_i from the Fourier amplitude spectrum (Fig. 4b) at integer multiples of the footfall rate f_r (in Hz, thus here also called "running frequency"). Commonly known as "dynamic load factors" (DLFs), α_i coefficients have been intensively studied for walking, jumping and bouncing [22] and the results have been incorporated in the most advanced vibration serviceability guidelines. On the other hand, values of the phase angles φ_i have never been publicised in detail and are usually ignored in Eq. (1).

A number of studies has shown that the Fourier modelling approach leads to significant loss of information and introduction of inaccuracies during the data reduction process [6,7,16,46,47]. For instance, Brownjohn et al. [46] reported differences as high as 50% between vertical vibrations of pedestrian structures due the imperfect real walking forces and periodic Fourier-based simulations, which were related to neglecting the energy around dominant harmonics in actual narrow band forces (Fig. 4b). Recent studies based on comparisons between the measured and simulated structural response due to the actual imperfect and artificial periodic pedestrian loading of footbridges [48] and floors [49], as well as due to jumping and bouncing loading of grandstands [50], all recognised the importance of modelling near-periodic nature of human-induced loads. Although a quality fit of the complete Fourier amplitude spectrum could be obtained, e.g. as suggested for the vertical walking forces elsewhere [2,46], widely varying harmonic phase lags φ_i (Figs. 4c and 5) are very difficult to characterise analytically. If they are, however, assumed to be uniformly distributed in the range $[-\pi, \pi]$, the sum of Fourier harmonics normally does not match the actual force time history. This is illustrated by comparison of Fig. 4a–d. Hence, randomising phases is not the way forward. They seem to be a structured data set rather than an assembly of uniformly distributed random numbers. This clearly demonstrates that the Fourier series can only provide rudimentary conceptualisation of individual running loads. However, fitting Eq. (1) to the numerous database of running force records established in Section 3 can provide a valuable insight into their inter-subject variability, which this paper specifically aims to address in Section 7. The results of the fitting are summarised in the next section.

5. Inter-subject randomness of running forces

Graphs shown in Fig. 6 indicate that running force amplitudes generally increase as people increase their footfall rate. Due to the apparently large scatter of the DLF values at a fixed running frequency their relationship cannot be described reliably as a deterministic function, such as the linear and polynomial curve fits suggested for vertical walking loads elsewhere [20,41,42]. Moreover, histograms of DLFs corresponding to a narrow range 0.1 Hz around the most frequent footfall rate in the sample $f_r = 2.7$ Hz do not resemble any known probability density function (Fig. 7), which is a key condition for probabilistic curve fitting [52]. The Kolmogorov–Smirnov (K–S) goodness of fit test [51] rejects the hypothesis (at 5% confidence level) that the DLF data come from a normal, lognormal, gamma, Rayleigh or exponential distribution

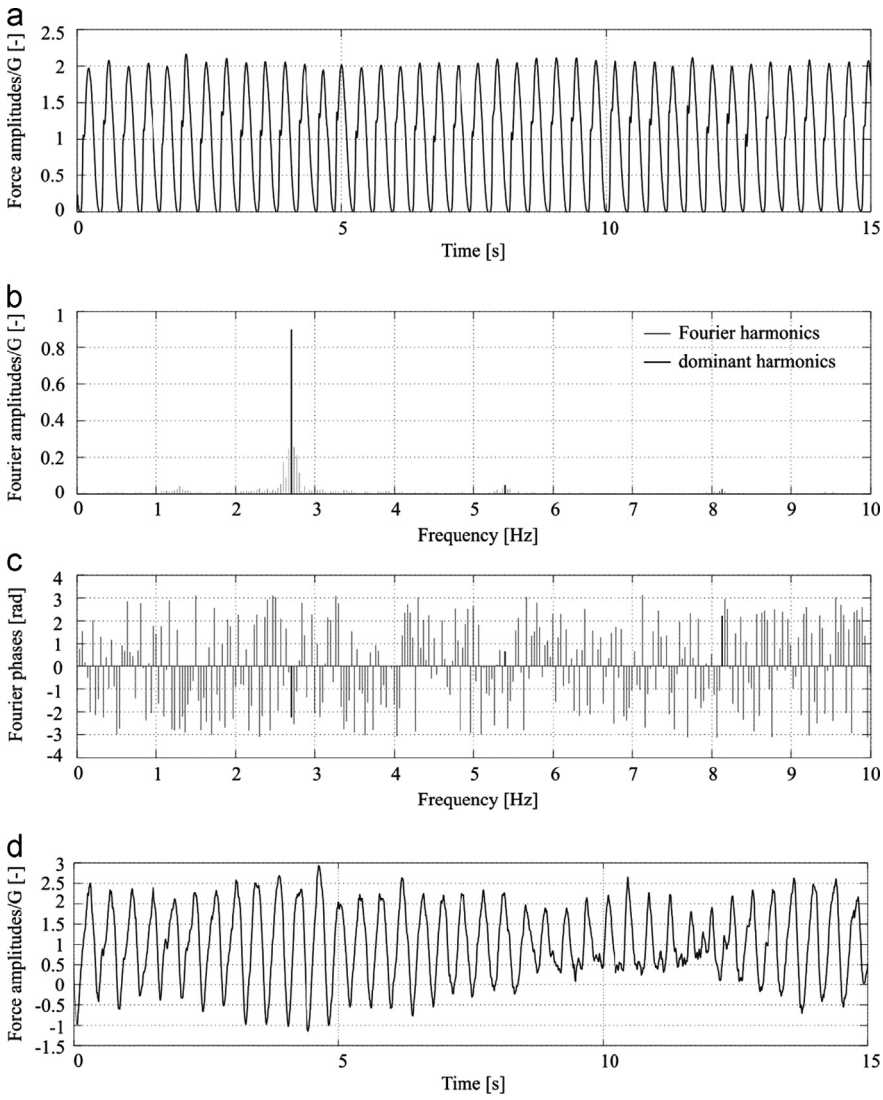

Fig. 4. (a) An example of continuously measured running force signal and the corresponding Fourier (b) amplitude and (c) phase spectra derived from 30 s long force–time history. (d) The force–time history reproduced using the amplitude spectrum shown in (b) and uniformly distributed phases in the range $[-\pi, \pi]$.

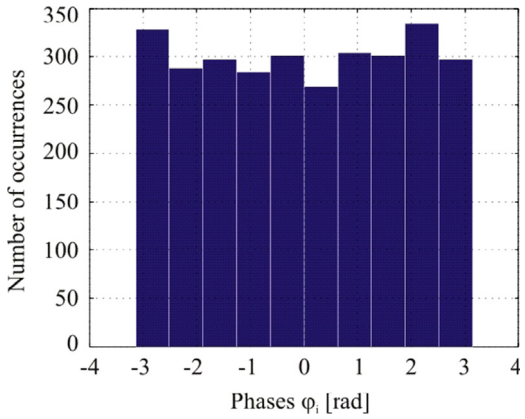

Fig. 5. Histogram of the phases illustrated in Fig. 4c.

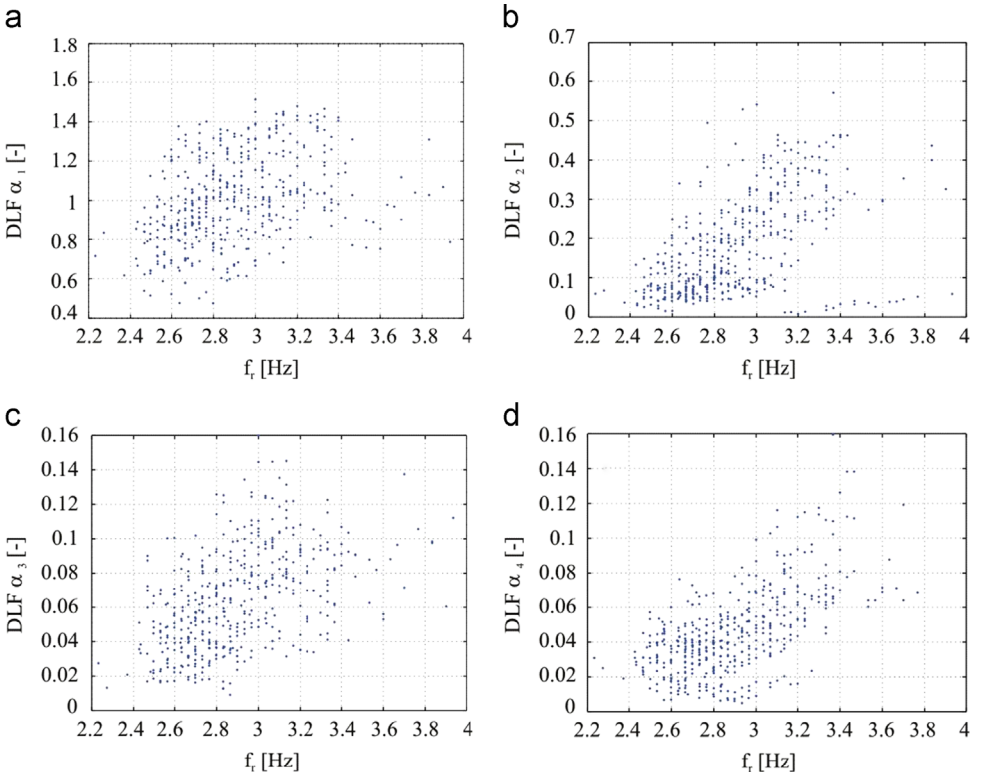

Fig. 6. Footfall rate *fr* vs. DLFs ($\rho a = 0.37$, $\rho b = 0.52$, $\rho c = 0.47$, $\rho d = 0.62$).

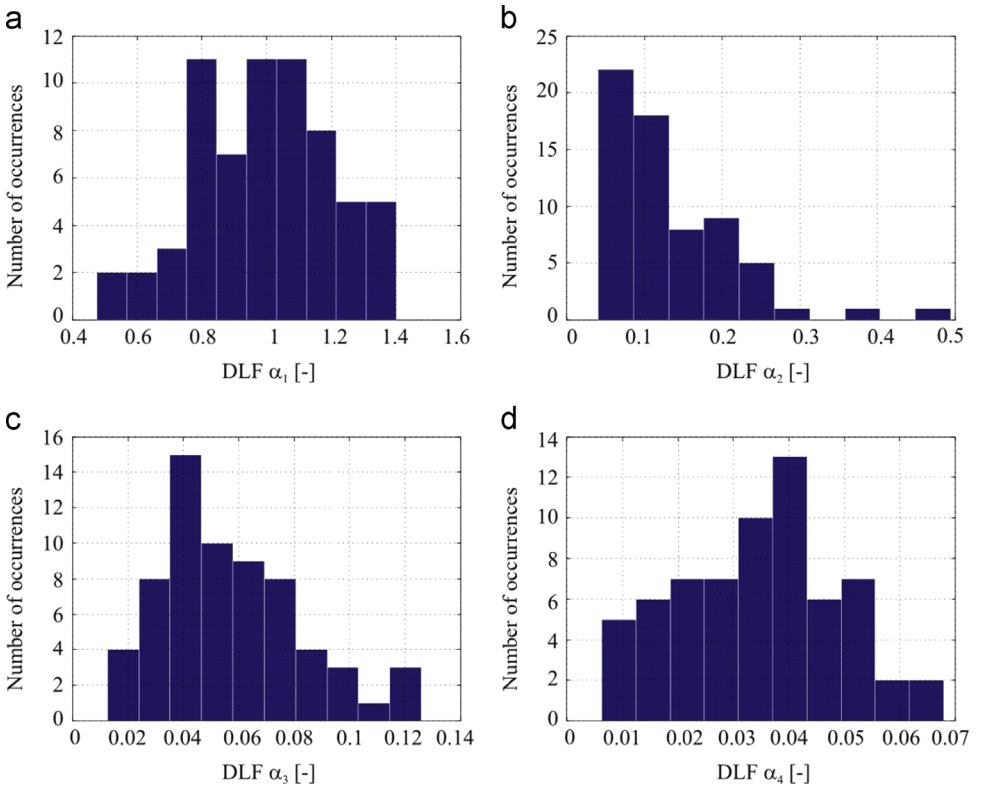

Fig. 7. Histograms of the first four DLFs in a narrow range 0.1 Hz around the most frequent footfall rate $fr = 2.70$ Hz.

Table 1
Results of Kolmogorov–Smirnov goodness of fit test (at 5% confidence level) corresponding to the data shown in Fig. 7.

p-value	Probability distribution				
	Normal	Lognormal	Gamma	Rayleigh	Exponential
DLF α_1	0.293	0.419	0.880	0.120	0.890
DLF α_2	0.419	0.880	0.219	0.408	0.071
DLF α_3	0.087	0.429	0.196	0.196	0.458
DLF α_4	0.196	0.087	0.126	0.293	0.781

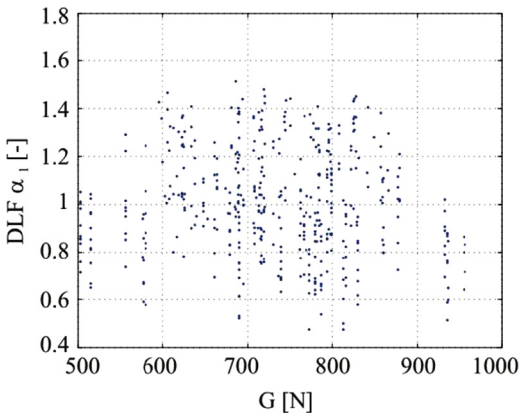

Fig. 8. Body weight *G* vs. DLF $\alpha 1$.

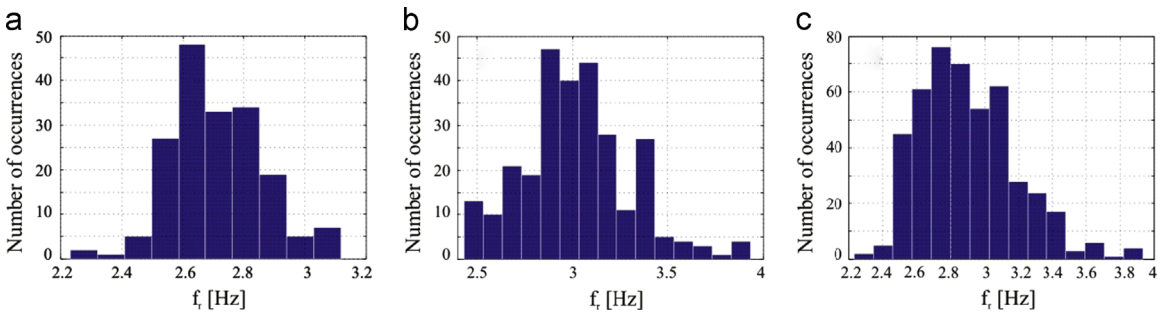

Fig. 9. Histograms of running footfall rates derived from the force signals recorded in (a) Sheffield, (b) Saint-Etienne, and (c) both Sheffield and Saint-Etienne.

(Table 1). Similar scatter in the histograms and outcome of the K–S test can also be observed for DLFs in the close proximity of fixed running speeds.

Fig. 8 proves that the body weight *G* and the fundamental DLF α_1 are uncorrelated variables ($\rho = -0.07$), indicating that the running style may be the single most important factor affecting amplitudes of running loads. As a result, arbitrary *G* values can be assigned to a synthetic *G*-normalised force signal as an independent random parameter. For instance, one can use probability density functions of the body weight, such as reported by Hermanussen et al. [53] for German, Austrian and Norwegian citizens, to generate random *G* values. This is an important aspect of the modelling strategy presented in Section 7.

Shapes of the histograms shown in Fig. 9 suggest that running footfall rate is not a normally distributed variable as in case of walking [2,13,47,54]. The normal probability plots in Fig. 10 and the results of the K–S test summarised in Table 2 further prove the point. Moreover, fitting a wide range of other probability density functions, such as the family of skewed distributions [52], showed a lack of statistical significance (Table 2).

Apart from the strong linear trend between running speed and footfall rate ($\rho = 0.75$), Fig. 11 illustrates a large scatter of the running frequencies at fixed running speeds, and vice versa. This observation can play a key role in simulating reliably running excitation of bridges due to dense crowd situations (e.g. marathon events) where running speed of individuals in a crowd can be imposed by spatial constrains and the crowd flow. As in the case of DLFs, visual inspection of the histograms in

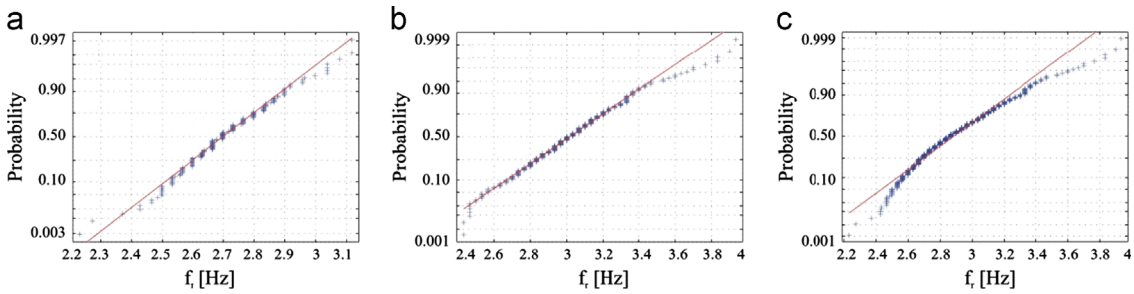

Fig. 10. Normal probability plots corresponding to the data shown in Fig. 9.

Table 2
Results of Kolmogorov–Smirnov goodness of fit test (5% confidence level) corresponding to the data shown in Fig. 9.

p-value	Probability distribution			
	Normal	Lognormal	Gamma	Rayleigh
Sheffield data	0.634	0.461	0.385	0.076
Saint-Etienne data	0.661	0.283	0.801	0.081
All	0.393	0.069	0.180	0.069

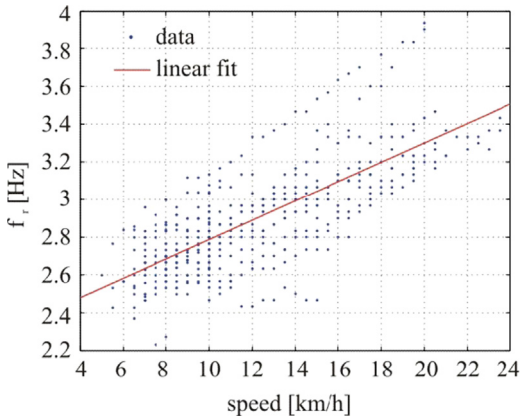

Fig. 11. Running speed vs. footfall rate (ρ=0.75).

Fig. 12 shows that distribution of the footfall rates at fixed running speeds cannot be approximated satisfactorily by any known probability density function.

The results presented so far have demonstrated large intra- and inter-subject randomness of running forces which cannot be modelled reliably using the popular deterministic Fourier series approach. To simulate more accurately the intra-subject variability of running, the next section offers a sophisticated modelling strategy featuring individual forces as a narrow band process. The inter-subject variability is addressed in Section 7, where the model is fitted to each of the 458 force records measured in Section 3 yielding a numerical generator of random narrow band running time series.

6. Modelling near-periodic force signals

Due to the naturally occurring variations in all repetitive human movements, the force measures vary on cycle-by-cycle basis. A running cycle can be defined between any two nominally identical events in the force–time history. In this study, the instant at which the feet hit the ground (also known as “initial contact”) leading to a new force pulse was selected as starting (and completing) event (Fig. 13).

From the 35 s long force signal (a fraction is shown in Fig. 13) and yielding about 94 cycles, a window comprising 76 successive cycles was extracted from the middle. Nine cycles (i.e. approximately 10% of all cycles measured) at the beginning and end of the force record were cast aside since their natural variability might be affected by the measuring process. In the next section, the selected 76 cycles are used to model morphology of the force signal (so called “template cycle”), while

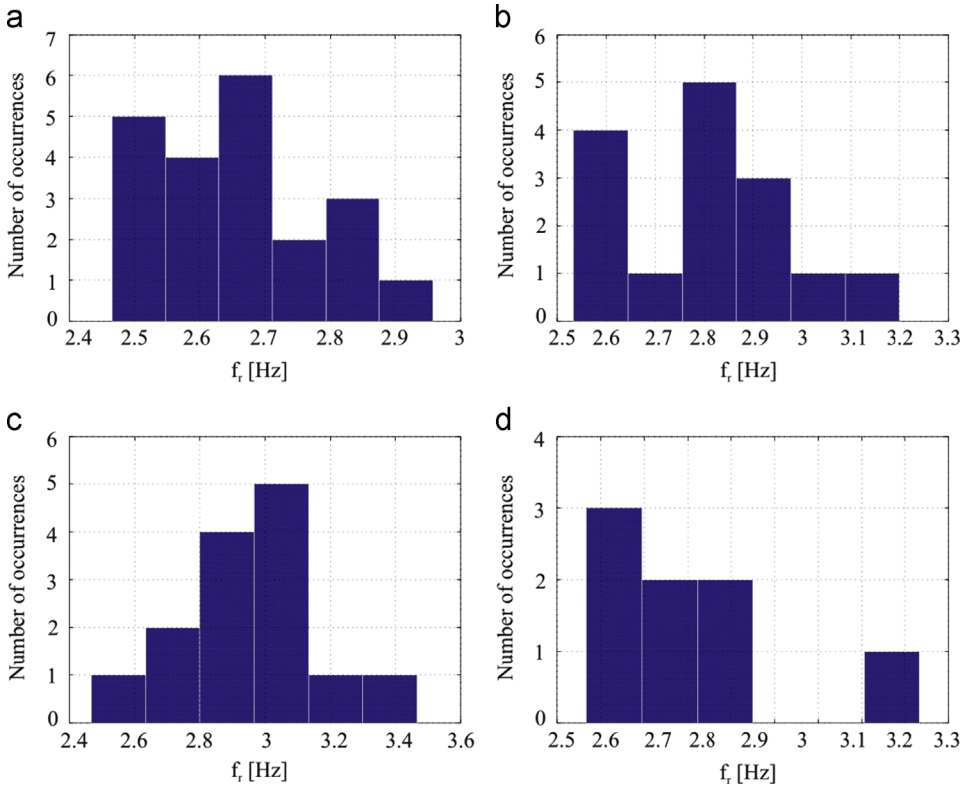

Fig. 12. Histograms of footfall rates at fixed running speeds (a) 7 km/h, (b) 11 km/h, (c) 15 km/h, and (d) 19 km/h.

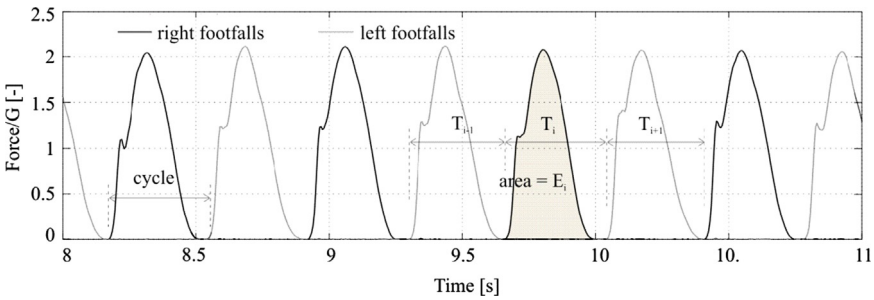

Fig. 13. A portion of a 35 s long force–time history ($fr = 2.70$ Hz).

modelling variability of the cycle intervals and force amplitudes is outlined in Sections 6.2 and 6.3. The models are motivated by an existing numerical generator of electrocardiogram (ECG) signals [44], which have similar near-periodic features as running time series. Section 6.4 illustrates how the template cycle can be scaled (i.e. stretched and compressed) on the cycle-by-cycle basis along the synthetic time and amplitude axes to reflect the intra-subject variability present in the actual force–time history.

6.1. *Template cycle*

The selected 76 cycles have been normalised by the body weight G, aligned to their starting points and resampled to the length of the longest cycle. Visual inspection of Fig. 14 suggests that there is a common waveform which distorts along time and amplitude axes on a cycle-by-cycle basis. Their average would be an inadequate representative of the force morphology due to misalignments of the common events, such as positions of the local extreme values. Hence, before finding the average (i.e. the template cycle) all selected cycles had been lined up using dynamic time warping (DTW) method. Originally developed for speech recognition, the DTW nonlinearly warps two discrete signals to align similar events along time dimension and thereby minimise the sum of squared differences [45]. This process is illustrated in Fig. 15a. In a similar way

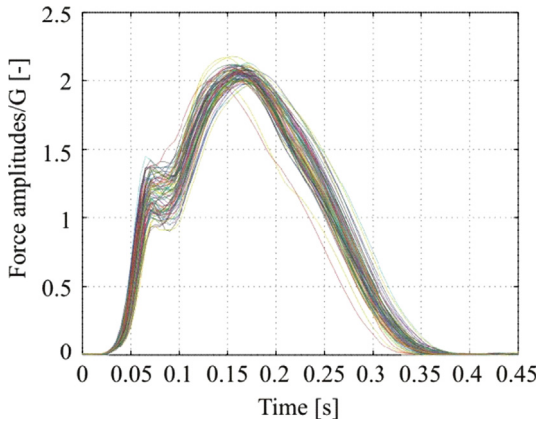

Fig. 14. Resampled *G*-normalised cycles for DTW.

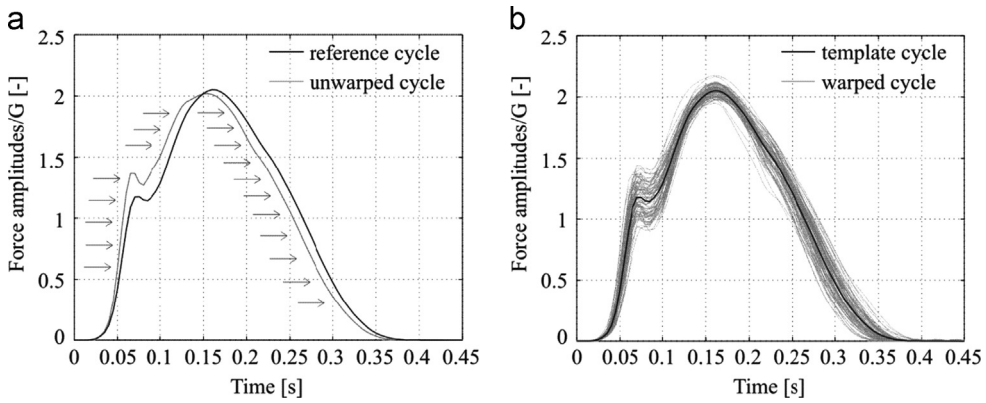

Fig. 15. (a) Illustration of DTW and (b) template cycle.

wavelet analysis linearly shifts and stretches so called "mother" wavelet [55]. However, due to the apparent nonlinear misalignments of the common events in the force data, linear shifting and stretching is considered unsuitable in this study.

The DTW is designed to warp only two trajectories at a time, so the cycles are warped individually onto a "reference cycle" (Fig. 15a). It is one of the measured cycles in Fig. 14 that minimises the sum of point-by-point Euclidiean distances to their simple numerical point-by-point average [56]. The resulting warped cycles and template cycle are shown together in Fig. 15b.

The underlying shape of the template cycle can be modelled mathematically as a sum of four Gaussian functions (Fig. 16 and Table 3):

$$Z(t) = \sum_{j=1}^{4} A_j \, e^{-(t-t_j)^2/2\delta_j^2} \tag{2}$$

where $Z(t)$ is the curve fit, the parameter A_j is the height (also called weight) of the jth Gaussian peak, t_j is the position of the centre of the peak, and δ_j controls the width of the Gaussian bell functions. The number of Gaussians in the sum and values of the parameters are optimised using nonlinear least-square curve fit [57].

6.2. Variability of cycle intervals

Variations of cycle intervals T_i ($i = 1, \ldots, 76$) can be represented by a dimensionless set of numbers τ_i:

$$\tau_i = \frac{T_i - \mu_T}{\mu_T}$$
$$\mu_T = mean(T_i) \tag{3}$$

As τ_i series has zero mean value, its variance is the integral of its auto spectral density (ASD) [55]. Assuming that the variation of τ_i does not change for the given test subject, footfall rate and duration of running, the ASD of the actual τ_i data can be used to generate synthetic series τ_k' ($k = 1, \ldots, N$) of arbitrary length (e.g. $N \gg 76$) with the same statistical properties, such as standard deviation and "pattern" of variation between successive τ_i values. Empirical evidence is provided in Section 6.4.

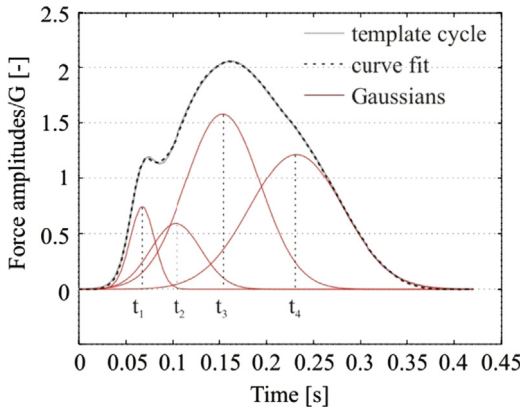

Fig. 16. Fitting the template cycle.

Table 3
Parameters of curve fit $Z(t)$.

Parameters	Coefficients (95% confidence intervals)			
	$j=1$	$j=2$	$j=3$	$j=4$
Aj	0.742 (0.639, 0.844)	0.592 (−0.122, 1.306)	1.582 (1.071, 2.093)	1.216 (1.018, 1.413)
t_j	0.0675 (0.0671, 0.0678)	0.1035 (0.0981, 0.1089)	0.1536 (0.1431, 0.1641)	0.2317 (0.2215, 0.2419)
δ_j	0.018 (0.017, 0.019)	0.038 (0.024, 0.052)	0.056 (0.042, 0.071)	0.070 (0.065, 0.075)

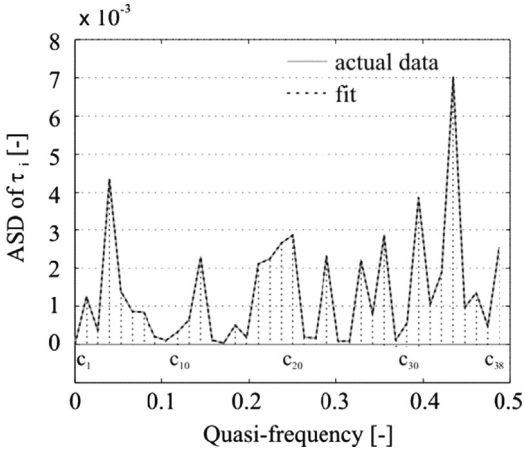

Fig. 17. ASD of τ_i series and its curve fit.

An ordinary random number generator, such as a probability density function of τ_i, cannot model the pattern as it cannot reflect the frequency content of τ_i series.

The ASD of τ_i can be calculated as [55]

$$S_\tau(f_m) = \frac{A_\tau^2(f_m)}{2\Delta f}, \quad f_m = \frac{m}{76}, \quad m = 0, \ldots, 37 \tag{4}$$

where $A_\tau(f_m)$ is a single-sided discrete Fourier amplitude spectra and $\Delta f = 1/76$ is the spectral line spacing (Fig. 17). The ASD ordinates do not depend on the number of discrete data points τ_i, but it is coarse due to their limited number. More points would result in a smoother ASD and might reveal a richer ASD structure but this requires more measured cycles. However, having longer force records would be ethically inappropriate. Guided by the Research Ethics Committees in the University of Sheffield and the University Jean Monnet Saint-Etienne the test duration was limited to avoid fatigue and discomfort, which can also influence natural variability of the force records.

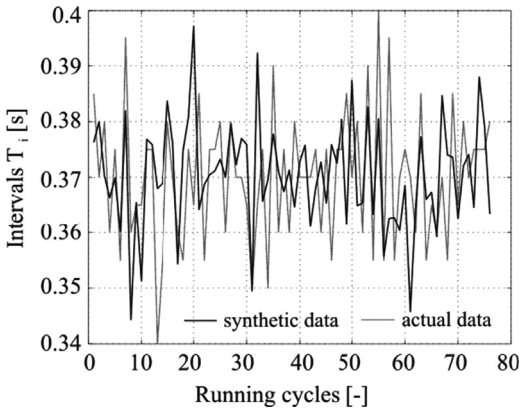

Fig. 18. Measured and an example of synthetic cycle intervals.

Similarly to the template cycle (Section 6.1), the ASD $S_\tau(f_m)$ can be mathematically described by a sum of 38 equidistant Gaussian functions (Fig. 17):

$$S_\tau'(f) = \sum_{j=1}^{38} W_j \, e^{-(f-c_j)^2/2b^2} \tag{5}$$

Here, parameter W_j is the height of the jth Gaussian peak, c_j is the position of the centre of the peak, and b is the common width of the Gaussian function. The Gaussian centres c_j are placed in each sample on the quasi-frequency axis to fit exactly the actual ASD (Fig. 17). For such fixed positions of c_j and predefined widths $b = \Delta f$, Gaussian heights W_j can be optimised using the nonlinear least-square method [57].

Generation of synthetic series τ_k' $(k = 0, \ldots, N)$ starts by calculating $S_\tau'(f_n)$ values using Eq. (5) at discretely spaced frequency points $f_n = n\Delta f'$, where $n = 0, \ldots, N/2-1$ and $\Delta f' = 1/N$. The synthetic ASD amplitudes are then used in conjunction with Eq. (4) to generate a set of Fourier amplitudes $A_\tau'(f_n) = \sqrt{2\Delta f' S_\tau'(f_n)}$. Finally, assuming random distribution of phase angles in the range $[-\pi, \pi]$, $A_\tau'(f_n)$ are used in inverse FFT algorithm to generate a set of N synthetic τ_k' values. Different τ_k' series with the same spectral properties can be synthesised by using different sets of the random phases obtained by varying the seed of the random number generator.

According to Eq. (2), scaling τ_k' by μ_T and adding the offset value μ_T, results in a series of synthetic intervals T_k' (Fig. 18). Assuming that the test subject does not vary significantly their running style in a narrow range of footfall rates, μ_T value can be slightly changed in the scaling process to generate cycle intervals at rates close to $1/\mu_T$. Empirical evidence is presented in Section 7.

6.3. Variability of force amplitudes

Energy of running cycles E_i can be defined as the integral of the G-normalised force amplitudes over the corresponding cycle intervals T_i (Fig. 13). Due to the fairly linear trend between these two parameters, it is possible to simulate the energy transfer between successive cycles using the following linear regression model (Fig. 19):

$$E_i = \rho_1 T_i + \rho_0 + \Delta E_i \tag{6}$$

Here, $\rho_1 = 0.498$ and $\rho_0 = 0.183$ are regression coefficients and ΔE_i is a disturbance term or error, which is usually modelled as a random Gaussian noise [52].

Given a set of synthetic cycle intervals T_k' $(k = 1, \ldots, N)$ generated as presented in Section 6.2, the corresponding synthetic series E_k' can be calculated using Eq. (6). These energies can be assigned to k template cycles by scaling their amplitudes by factors ξ_k:

$$\xi_k = \frac{E_k'}{E_{tc}} \tag{7}$$

where E_{tc} is the energy of the template cycle. When sequenced along the time axis, the scaled template cycles also reflect the variation of the force amplitudes on a cycle-by-cycle basis, as illustrated in Fig. 20.

6.4. Synthetic force signals

Visual comparison of Fig. 20a to b and Fig. 21a to 20b shows the apparent similarity between the measured signal and an example of synthetic force signal in both time and frequency domain.

Two identical synthetic force signals can be generated only by chance since the modelling parameters T_k' and $\Delta E_k'$ are random variables. However, a family of synthetic forces share three key properties inherited from the measured signal:

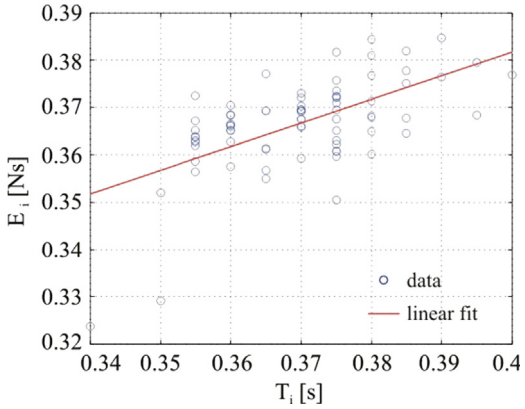

Fig. 19. Cycle energy *Ei* vs. cycle intervals *Ti*.

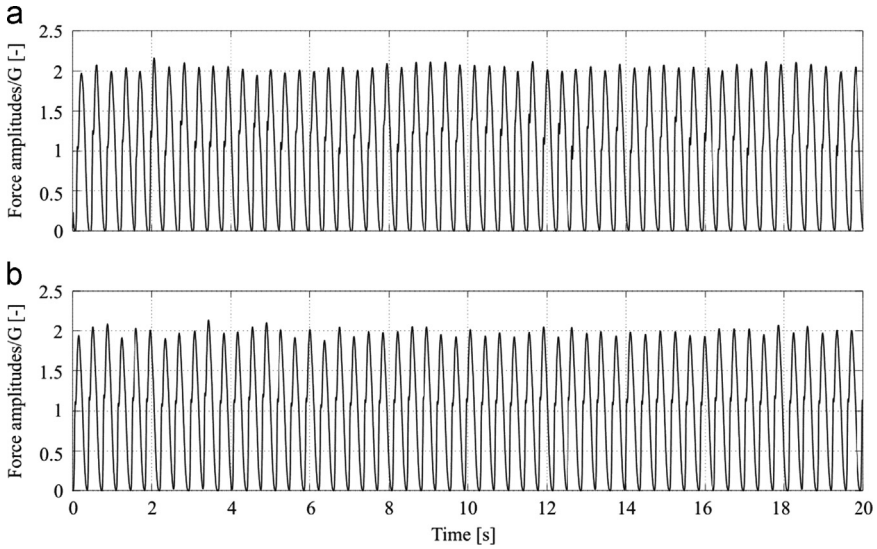

Fig. 20. (a) Measured and (b) an example of synthetic force–time series.

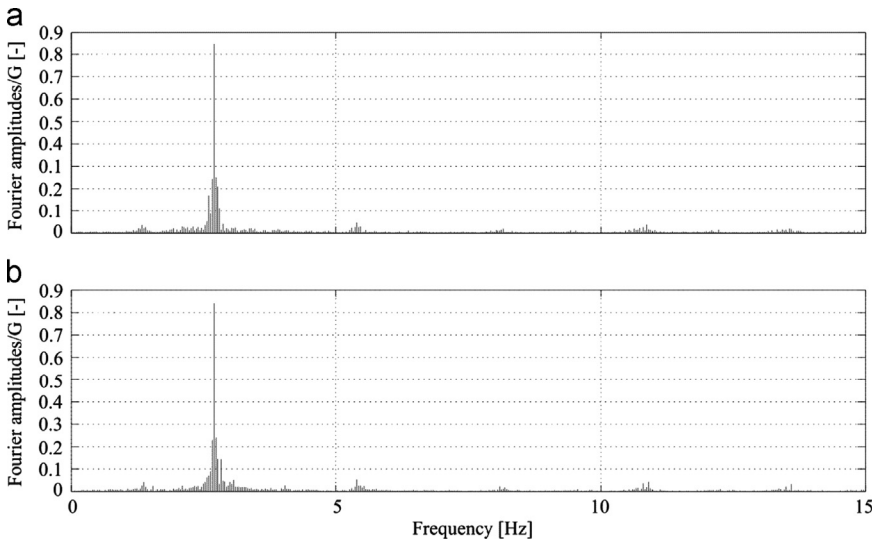

Fig. 21. Discrete Fourier amplitude spectra of the time series shown in Fig. 20.

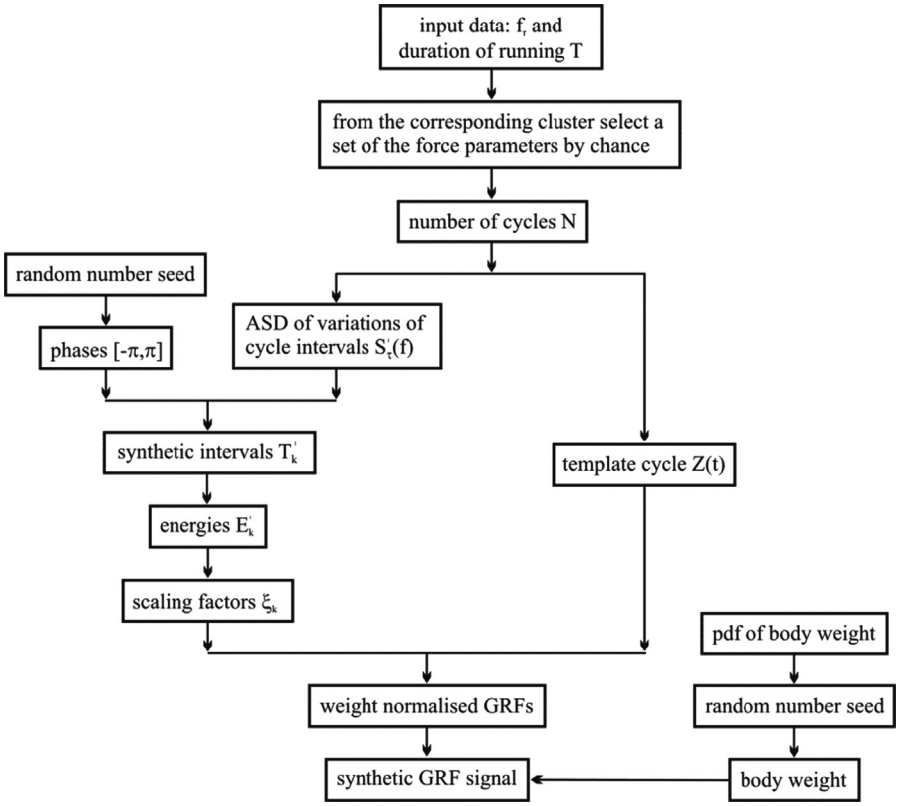

Fig. 22. Flow chart illustrating generating of artificial force signals.

(1) Shapes of the running footfalls are drawn from the same template cycle.
(2) Cycle intervals $T_k^{'}$ are statistically equivalent since they share the same ASD.
(3) According to Eq. (6), the statistical equivalence of $T_k^{'}$ series reflects directly equivalence of $E_k^{'}$ energies.

The next section shifts focus of the study from intra- to inter-subject variability. It integrates the numerous database of individual force records established in Section 3, the knowledge on their randomness presented in Section 5 and their mathematical characterisation outlined in Section 6, to create a numerical generator of random narrow band running time series.

7. Numerical generator of random artificial force signals

Each of the 458 force records in the database established in Section 3 was processed using the concept described in Section 6. Multiple sets of information, such as parameters of the template cycle $Z_k(t)$, the ASD $S_\tau^{'}(f)$, disturbance term $\Delta E_i(t)$ and the regression coefficients ρ_1 and ρ_0, were extracted and stored in 458 MATLAB structure files ([58]). These are called "mat files" in the remaining part of the paper.

The mat files were classified into 15 clusters with respect to the running footfall rate, as shown in the histogram in Fig. 9c. Each bar in the histogram is only 0.1 Hz wide, thus it is reasonable to assume that any mat file in a cluster can be used to generate synthetic signals at any footfall rate within the cluster's narrow frequency range. This implies that the modelling parameters extracted from the actual force measurements with a certain footfall rate can be used to generate artificial force signals at close rates. This is a key feature of the random modelling strategy adopted in this section.

The flow chart in Fig. 22 outlines the algorithm of creating synthetic force signals. For specified footfall rate f_r and duration of running excitation G the algorithm first calculates the total number of running cycles N in the force signal. Then, from a cluster corresponding to the f_r, it selects randomly and equally likely a mat file. Using the information about the ASD function $S_\tau^{'}(f)$ stored in the file, the algorithm generates synthetic cycle intervals $T_k^{'}$, $k = 1, \ldots, N$, as elaborated in Section 6.2. These are further used to calculate the corresponding scaling factors ξ_k using Eqs. (6) and (7).

Having generated $T_k^{'}$ and ξ_k values, the template cycle $Z(t)$ is stretched and compressed along time and amplitude axes through N iterations, yielding weight normalised running forces of a kind shown in Fig. 20b. Finally, these become equivalent running force time histories when their amplitudes are additionally multiplied by a random body weight.

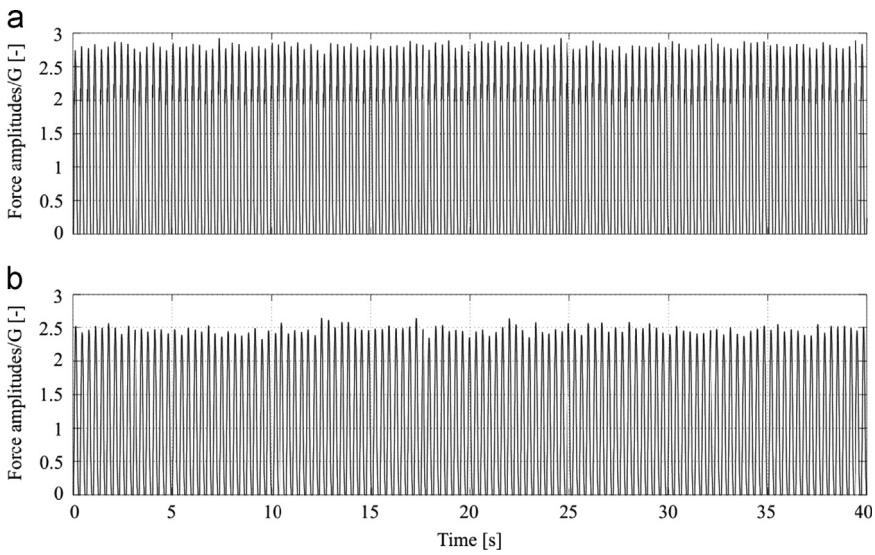

Fig. 23. Examples of artificial force signals generate for the same set of input parameters $fr = 3$ Hz and $T = 40$ s.

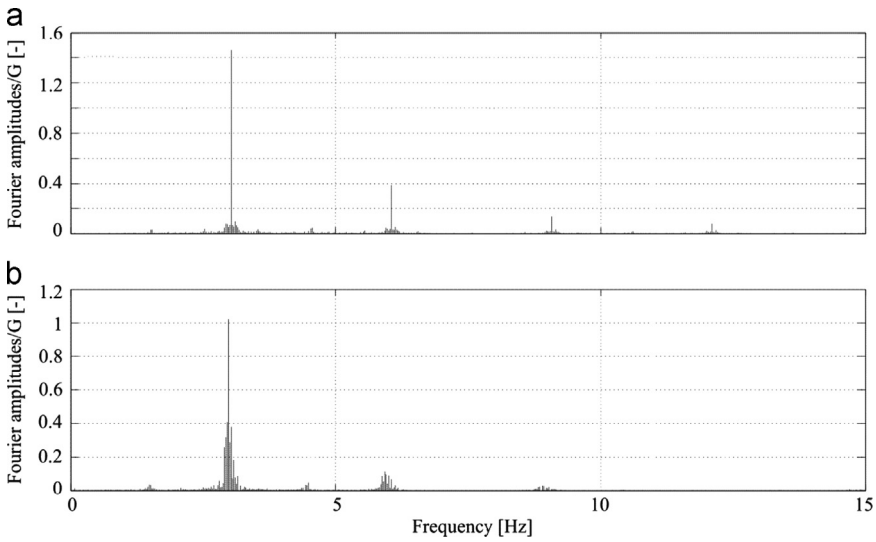

Fig. 24. Discrete Fourier amplitude spectra of the time series shown in Fig. 23.

Fig. 23 illustrates examples of force signals generated when the model was run twice in succession using the same input parameters: $f_r = 3$ Hz and $T = 40$ s. A visual comparison of the time series provides empirical evidence that the model accounts for the inter-subject variability. On the other hand, the ability to generate different degrees of the intra-subject variability is more obvious from comparison between the corresponding frequency spectra (Fig. 24). Greater "leaking" of energy around dominant harmonics in Fig. 24b relative to Fig. 24a indicates that the force signal in Fig. 23b is characterised by a greater degree of variability in amplitude and timing on the cycle-by-cycle basis.

8. Discussions and conclusions

The lack of fundamental forcing data and their reliable mathematical characterisation are the key reasons for a total lack of urgently needed formal design guidance regarding running excitation of bridges. To change this situation, this interdisciplinary study first established a unique database comprising 458 individual force signals collected from 45 individuals running on two biomedical instrumented treadmills at a wide range of speeds. Then, two attempts were made to mathematically describe the measurements. The first model featuring Fourier series was transferred and adopted from a popular contemporary design guideline on dynamic loads due to pedestrians walking. Based on the deterministic and perfectly periodic representation of human locomotion, this modelling approach was shown to oversimplify the actual running force signals since they are characterised by significant inter- and intra-personal randomness. The key intellectual

delivery of this study is a more comprehensive and robust data-driven mathematical model designed to generate random signals which can replicate both temporal and spectral features of the measured forces. The modelling strategy is motivated by the existing models of human electrocardiogram (ECG) signals and speech recognition, as well as stochastic models of wind and earthquake loading. Being derived from the force data recorded on stiff treadmills, the current version of the model represents reliably only individual running excitation of structures which do not vibrate perceptibly, i.e. cases when the ground reaction forces are not significantly affected by the structural vibrations. However, the model is an essential prerequisite for future quality models of dynamic loading induced by individuals and multiple runners under a wider range of conditions. From the structural engineer's point of view, there is still a gap in the knowledge on the proportion of individuals in a group or crowd who coordinate their body motion and the scale and character of the resulting net dynamic loads on the structure, with or without influence of the motion of the structure itself. In fact, perceptible motion of the structure is just one type of cue or stimulus among several others affecting human-induced loads, such as different auditory, visual and tactile stimuli. To include all these parameters in the model, the variations in the force amplitudes, energy, timing and shape for successive running cycles should be modelled as a function of bridge dynamic response, human perception to vertical vibrations and different external stimuli. To the best knowledge of the authors, experimental data necessary to accomplish this challenge is currently not available anywhere in the world.

When compared to the state-of-the-art approach to vibration serviceability design of bridges based on the Fourier series models, the key novelties and advantages of the proposed model are:

(1) There is a very little to choose between measured and artificially generated force signals. The model presented accounts for the near-periodic nature of running loads by simulating natural variability of timing, amplitudes and energy of the successive running footfalls, thus offers a more realistic and less conservative vibration serviceability assessment of bridges.
(2) The forces are described as a random rather than deterministic process, similar to other random excitation of civil engineering structures, such as due to wind, waves or earthquakes.
(3) The modelling strategy is numerically too complex to generate artificial forces manually, but it can be coded and distributed to structural designers as computer software. This offers a great potential to modernise the vibration serviceability assessment by shifting from traditional hand calculations towards fully computerised design. Moreover, as the model generates synthetic force signals in a fraction of a second even on a standard office PC configuration, the software would enable more efficient and cost-effective structural design.

Acknowledgements

The authors would like to acknowledge the financial support provided by the UK Engineering and Physical Sciences Research Council (EPSRC) for Grant reference EP/E018734/1 (“Human Walking and Running Forces: Novel Experimental Characterisation and Application in Civil Engineering Dynamics”) and to thank all test subjects for participating in the data collection.

References

[1] M. Black, G. Webster, Jane Coston Cycle bridge: a model for managing vibration, Proc. ICE – Civil Eng. 159 (3) (2009) 120–125.
[2] S. Zivanovic, A. Pavic, P. Reynolds, Probability-based prediction of multi-mode vibration response to walking excitation, Eng. Struct. 29 (6) (2007) 942–954.
[3] T. Fitzpatrick, P. Dallard, S. Le Bourva, A. Low, R. Ridsdill-Smith, M. Willford, Linking London: the Millennium Bridge, The Royal Academy of Engineering, London, UK, 2001 (Report no. L12.32).
[4] S. Nakamura, Field measurements of lateral vibration on a pedestrian suspension bridge, Struct. Eng. 81 (22) (2003) 22–26.
[5] J.M.W. Brownjohn, P. Fok, M. Roche, P. Mayo, Long span steel pedestrian bridge at Singapore Changi Airport. Part 2: crowd loading tests and vibration mitigation measures, Struct. Eng. 82 (16) (2004) 28–34.
[6] S. Zivanovic, A. Pavic, P. Reynolds, Human–structure dynamic interaction in footbridges, Bridge Eng. 158 (BE4) (2005) 165–177.
[7] S. Zivanovic, A. Pavic, P. Reynolds, Vibration serviceability of footbridges under human-induced excitation: a literature review, J. Sound Vib. 279 (2005) 1–74.
[8] J.H.G. Macdonald, Pedestrian-induced vibrations of the Clifton Suspension Bridge, Pro. Inst. Civ. Eng. Struct. Build. 161 (2008) 69–77.
[9] M. Kasperski, C. Sahnaci, Serviceability of pedestrian structures exposed to vibrations during marathon events, in: Proceedings of IMAC XXVI, Orlando, FL, USA, 4–7 February 2008.
[10] E. Caetano, A. Cunha, C. Moutinho, Vandal loads and induced vibrations on a footbridge, ASCE J. Bridge Eng. 16 (3) (2011) 375–382.
[11] J.H.G. Macdonald, Lateral excitation of bridges by balancing pedestrians, Proc. R. Soc. A (2008). (16 December).
[12] F. Venuti, L. Bruno, The synchronous lateral excitation phenomenon: modelling framework and an application, C. R. Mec. 335 (2007) 739–745.
[13] E.T. Ingólfsson, C.T. Georgakis, F. Ricciardelli, J. Jönsson, Experimental identification of pedestrian-induced lateral forces on footbridges, J. Sound Vib. 330 (6) (2011) 1265–1284.
[14] V. Racic, A. Pavic, Stochastic approach to modelling near-periodic jumping force signals, Mech. Syst. Signal Process. 24 (2010) 3037–3059.
[15] F.W. Galbraith, M.V. Barton, Ground loading from footsteps, J. Acoust. Soc. Am. 48 (5) (1970) 1288–1292.
[16] J.H. Rainer, G. Pernica, D.E. Allen, Dynamic loading and response of footbridges, Can. J. Civ. Eng. 15 (1) (1988) 66–71.
[17] C. Sahnaci, M. Kasperski, Excitation of buildings and pedestrian structures from walking and running, in: Proceedings of EVACES07, Porto, Portugal, 24–26 October 2007.
[18] A. Belli, P. Bui, A. Berger, J.R. Lacour, A treadmill for measurements of ground reaction forces during walking, in: Proceedings of the XVth Congress of the International Society of Biomechanics, Jyväskylä, Finland, July 1995, pp. 100–101.

[19] K. Sabri, M.E. Badaoui, F. Guillet, A. Belli, G. Millet, J.B. Morin, Cyclostationary modeling of ground reaction force signals, Signal Process. 90 (4) (2010) 1146–1152.
[20] A. Pavic, M. Willford, Vibration serviceability of post-tensioned concrete floors, Appendix G, in: Post-tensioned Concrete Floors Design Handbook, Technical Report 43, 2005, pp. 99–107.
[21] T.A. McMahon, P.R. Greene, The influence of track compliance on running, J. Biomech. 12 (1979) 893–904.
[22] V. Racic, A. Pavic, J.M.W. Brownjohn, Experimental identification and analytical modelling of human walking forces: literature review, J. Sound Vib. 326 (2009) 1–49.
[23] J.K. DeWitt, R.L. Cromwell, R.D. Hagan, The effect of manipulating subject mass on ground reaction force during locomotion, in: Proceedings of the American Society of Biomechanics Annual Meeting, Blacksburg, USA, September 2006.
[24] T.A. McMahon, G. Valiant, E.C. Frederick, Groucho running, J. Appl. Physiol. 62 (1987) 2326–23337.
[25] M. Fritz, K. Peikenkamp, Simulation of the influence of surfaces on measured vertical ground reaction forces during fast movements, in: D. De Waard, K.A. Brookhuis, S.M. Sommer, W.B. Verwey (Eds.), Human Factors in the Age of Virtual Reality, Shaker Publishing, Maastricht, The Netherlands, 2003, pp. 233–235.
[26] M.A. Nurse, M. Hulliger, J.M. Wakeling, B.M. Nigg, D.J. Stefanyshyn, Changing the texture of footwear can alter gait patterns, J. Electromyogr. Kinesiol. 15 (2005) 496–506.
[27] T.S. Keller, A.M. Weisberger, J.L Ray, S.S. Hasan, R.G. Shiavi, D.M. Spengler, Relationship between vertical ground reaction force and speed during walking, slow jogging, and running, Clin. Biomech. 11 (5) (1996) 253–259.
[28] H.J. Ralston, Energetics of human walking, in: R.M. Herman, S. Grillner, P.S.G. Stein, D.G. Stuart (Eds.), Neural Control of Locomotion, Plenum Press, New York, 1976, pp. 77–98.
[29] M. Srinivasan, A. Ruina, Computer optimisation of a minimal biped model discovers walking and running, Nature 439 (2006) 72–75.
[30] R. Margaria, Biomechanics and Energetics of Muscular Exercise, Clarendon, Oxford, UK, 1977.
[31] A. Thorstensson, H. Robertson, Adaptations to changing speed in human locomotion: speed of transition between walking and running, Acta Physiol. Scand. 131 (1987) 211–214.
[32] A.E. Minetti, L.P. Ardigo, F. Saibene, The transition between walking and running in humans: metabolical aspects at different gradients, Acta Physiol. Scand. 150 (1994) 315–323.
[33] W.C. Scott, H.J. Yack, C.A. Tucker, H.Y. Lin, Comparison of vertical ground reaction forces during overground and treadmill walking, Med. Sci. Sports Exerc. 30 (10) (1988) 1537–1542.
[34] R.C. Nelson, C.J. Dillman, P. Lagasse, P. Bickett, Biomechanics of overground versus treadmill running, Med. Sci. Sports 4 (4) (1972) 233–240.
[35] M. van de Putte, N. Hagemeister, N. St-Onge, G. Parent, J.A. de Guise, Habituation to treadmill walking, Bio-Med. Mater. Eng. 16 (2006) 43–52.
[36] P.O. Riley, G. Paolini, U. Della Croce, K.W. Paylo, D.C. Kerrigan, A kinematic and kinetic comparison of overground and treadmill walking in healthy subjects, Gait Posture 26 (2007) 17–24.
[37] R. Bartlett, Introduction to Sports Biomechanics, 2nd ed. Routledge, London, UK, 2007.
[38] S. Bailey, Athlete First: A History of the Paralympic Movement, John Eiley & Sons, Chichester, UK, 2008.
[39] Kistler, Kistler User Manuals, 2013 ⟨www.kistler.com⟩.
[40] HEF Medical Development, ADAL3D User Manuals, ⟨http:/www.medical-development.com/home/default.asp⟩, 2013.
[41] P. Young, Improved floor vibration prediction methodologies, in: Proceedings of ARUP Vibration Seminar, London, UK, 4 October 2001.
[42] P. Young, Improved floor vibration prediction methodologies, in: Proceedings of ARUP Vibration Seminar, 4 October 2001, London, UK.
[43] A.K. Chopra, Dynamics of Structures: Theory and Applications to Earthquake Engineering, 4th ed, Prentice-Hall, Englewood Cliffs, NJ, USA, 2012.
[44] P.A. McShrry, G.D. Clifford, L. Tarassenko, L.A. Smith, A dynamical model for generating synthetic electrocardiogram signals, IEEE Trans. Biomed. Eng. 50 (2003) 289–294.
[45] J.R. Holmes, W. Holmes, Speech Synthesis and Recognition, 2nd ed, Taylor and Francis, London, UK, 2001.
[46] J.M.W. Brownjohn, A. Pavic, P. Omenzetter, A spectral density approach for modelling continuous vertical forces on pedestrian structures due to walking, Can. J. Civ. Eng. 31 (2004) 65–77.
[47] V. Racic, J.M.W. Brownjohn, Stochastic model of near-periodic vertical loads due to humans walking, Adv. Eng. Inf. 25 (2) (2011) 259–275.
[48] K. van Nimmen, P. van den Broeck, G. Lombaert, G. de Roeck, Characterisation of walking loads from inertial motion tracking, in: Proceedings of the Fourth International Conference on Computational Methods and Earthquake Engineering COMPDYN 2013, Kos, Greece, 12–14 June 2013.
[49] C.J. Middleton, Dynamic performance of high frequency floors (Ph.D. thesis), University of Sheffield, UK, 2009.
[50] J.H.H. Sim, A. Blakeborough, M. Williams, Statistical model of crowd jumping loads, ASCE J. Struct. Eng. 134 (12) (2008) 1852–1861.
[51] A. Justel, D. Peña, R. Zamar, A multivariate Kolmogorov–Smirnov test of goodness of fit, Stat. Probab. Lett. 35 (3) (1997) 251–259.
[52] C.M. Bishop, Pattern Recognition and Machine Learning, 4th ed, Springer, New York, USA, 2006.
[53] M. Hermanussen, H. Danker-Hopfe, G.W. Weber, Body weight and the shape of the natural distribution of weight, in very large samples of German, Austrian and Norwegian conscripts, Int. J. Obes. 25 (2001) 1550–1553.
[54] Y. Matsumoto, T. Nishioka, H. Shiojiri, K. Matsuzaki, Dynamic design of footbridges, IABSE Proceedings no. P-17/78, 1978, pp. 1–15.
[55] D.E. Newland, An Introduction to Random Vibrations, Spectral and Wavelet Analysis, 3rd ed, Pearson Education Limited, Harlow, UK, 1993.
[56] I.G.D. Strachan, Novel probabilistic algorithms for dynamic monitoring of Electrocardiogram waveforms, in: Proceedings of the Sixth International Conference on Condition Monitoring and Machinery Failure Prevention Technologies, 2009, pp. 545–555.
[57] D.M. Bates, D.G. Watts, Nonlinear Regression and its Applications, Wiley, New York, USA, 1998.
[58] MathWorks, Matlab User Guides, 2013, ⟨www.mathworks.com⟩.